International Journal of Thermal Sciences 49 (2010) 844–857

Contents lists available at ScienceDirect

International Journal of Thermal Sciences

journal homepage: www.elsevier.com/locate/ijts

Effect of cathode channel dimensions on the performance of an air-breathing PEM fuel cell

P. Manoj Kumar*, Ajit Kumar Kolar

Heat Transfer and Thermal Power Laboratory, Department of Mechanical Engineering, Indian Institute of Technology Madras, Chennai 600036, India

ARTICLE INFO

Article history:
Received 25 March 2009
Received in revised form
24 October 2009
Accepted 3 December 2009
Available online 31 December 2009

Keywords:
PEM fuel cell
Air-breathing
Performance
Cathode channel dimensions
Cell characteristics

ABSTRACT

A three dimensional, steady state, non-isothermal, single phase model was developed and simulations were carried out in order to find the effect of cathode channel dimensions (width, depth and height) on the performance of an air-breathing fuel cell. The model was solved using commercial CFD package Fluent (version 6.3). Separate user defined functions were written to solve the electrochemical equations and the water transport through the membrane along with the other governing equations. Analyses were carried out for three different channel widths (2, 4 and 6 mm), for three different channel depths (2, 6 and 10 mm) and for three different cell heights (15, 30 and 45 mm). Cell characteristics like current distribution, species distribution, oxygen mass transfer coefficient, cell temperature, cathode channel velocities and net water transport coefficients are reported. The results show that the cell performance improves with increase in cathode channel width, channel depth and with decrease in cell height. Maximum power density obtained was 240 mW/cm^2 for a channel width of 4 mm and channel depth of 6 mm. When the channel depth was 2 mm the performance was limited mainly due to the resistance offered by the channel for the buoyancy induced flow. For channel depths higher than 2 mm, the diffusion resistance of the porous GDL also contributed significantly to limit the performance to low current densities. At low current densities the fuel cell is prone to flooding whereas at high current densities ohmic overpotential due to dehydration of the membrane significantly contributes to the overall voltage loss.

1. Introduction

Cells that take up oxygen, for the cathode reaction, from ambient air by passive means are known as “air-breathing” fuel cells. In an air-breathing fuel cell, air flow along the cathode surface take place because of concentration and temperature gradient between the cell and the ambient. Air-breathing fuel cells have great potential as power source for low power portable electronic devices as it eliminates the use of compressor/blower and humidifier on the cathode side, thus making the system simple, light and compact.

Limited studies, both numerical and experimental, are available on the various factors that affect the performance of an air-breathing fuel cell such as ambient conditions [1–11], cathode structure and MEA properties [7–19], cell orientation [15–20], anode operating conditions [15,21,22], and long term operation [17,19,23] of the fuel cell. Few studies have been reported on the performance of air-breathing stack [24–26].

Since an air-breathing fuel cell take up oxygen, by natural convection, directly from the surrounding air, the ambient conditions play a very important role on the cell performance. Therefore most of the studies done so far have concentrated on the effect of ambient conditions on the cell performance. Another important factor that affects the cell performance is the cathode design. There are basically two different cathode designs that are widely used for air-breathing fuel cells, channel (ducted) and planar (ribbed). Most of the studies till now have concentrated on the planar fuel cell design. Experimental and modeling studies available in literature on channel cathode design are very few. Channel cathode design is important as they are more suitable for building air-breathing fuel cell stacks.

Mennola et al. [27] developed a two dimensional, isothermal and steady state model for the cathode side of the fuel cell. From the mass fraction distribution of water vapor they could conclude the formation of liquid water inside the cell and hence the importance of developing a two-phase model for better prediction of the results. Ying et al. [13] developed a two dimensional, steady state, single phase model of a complete fuel cell and from their studies they concluded that the channel width and rib width has to be

* Corresponding author. Fax: +91 44 2257 4652.
E-mail address: manoj_kp@iitm.ac.in (P. Manoj Kumar).

1290-0729/$ – see front matter © 2009 Elsevier Masson SAS. All rights reserved.
doi:10.1016/j.ijthermalsci.2009.12.002

Nomenclature

a	activity
c_p	specific heat (J kg^{-1} K^{-1})
C_w	molar concentration of water (mol m^{-3})
D	diffusivity (m^2 s^{-1})
E	Nernst voltage (V)
Eo	Nernst voltage at standard conditions (V)
F	Faradays constant (96 485 C mol^{-1})
g	Acceleration due to gravity (9.81 m s^{-2})
GDL	Gas Diffusion Layer
h_m	mass transfer coefficient (m s^{-1})
I	current density (A m^{-3})
I_o	exchange current density (A m^{-3})
J	mass flux (kg m^{-2} s^{-1})
k	thermal conductivity (W m^{-1} K^{-1})
M	molecular weight (kg mol^{-1})
$\dot{m}$	mass flux (kg m^{-2} s^{-1})
n	number of electrons transferred
n_d	net drag coefficient
P	pressure (N m^{-2})
R	universal gas constant (8.314 J mol^{-1} K^{-1})
R_{cell}	cell resistance (ohm-m^2)
S	entropy (J kg^{-1} K^{-1})
S_m	source term for continuity (kg m^{-3} s^{-1})
S_{mom}	source term for momentum (N m^{-3})
S_h	source term for energy (W m^{-3})
S_i	source term for species (kg m^{-3} s^{-1})
t	thickness (m)
T	temperature (K)
V	cell voltage (V)
v	velocity
Y	mass fraction

Greek symbols

α	net water transport coefficient
α_c	cathode charge transfer coefficient
β	permeability (m^2)
ρ	density (kg m^{-3})
μ	viscosity (m^2 s^{-1})
ε	porosity
λ	water content in the membrane
σ	conductivity (S m^{-1})

Subscripts

a	anode
act	activation
amb	ambient
c	cathode
cat	catalyst
conc	concentration
gdl	gas diffusion layer
H_2	hydrogen
H_2O	water vapor
lim	limiting
mem	membrane
mix	mixture
O_2	oxygen
oc	open circuit
sat	saturation

optimized for the best performance of the cell. They also developed a three dimensional, steady state, single phase model and validated the model with experiments [3,28]. They reported different cell characteristics at a constant current density of 150 mA/cm^2. Wang and Ouyang [30] gave a numerical expression for calculating Sherwood number as a function of Grashof number and diffusional Grashof number. Rajani and Kolar [5] developed a two dimensional, non-isothermal, steady state, single phase model for an air-breathing fuel cell with ducted cathode. They used the model to study the effect of ambient conditions on the cell performance. Effect of operating conditions on the performance of an air-breathing fuel cell was studied by Manoj and Kolar [6] from which they concluded that cathode conditions significantly affects the cell performance as compared to that of anode operating conditions. Tabe et al. [16] conducted experiments to study the effect of cathode structure on the cell performance. They conducted experiments with cells of planar and ducted cathode structure and their results shows that the cell performance is better with ducted cathode. Their results show that the channel dimensions significantly affects the cell performance and is the basis of the present work. Matamoros and Bruggeman [29] developed a three dimensional, non-isothermal model and their results show that cell performance is mainly limited due to slow oxygen transport to the active sites at low current densities and at current densities above 0.15 A/cm^2 ohmic overpotential also significantly contributes to the performance loss.

In a channel cathode fuel cell design, the channel dimensions play an important role on the performance of an air-breathing fuel cell. In this paper the effect of channel width, depth and height on the cell performance is studied with the help of a three dimensional model developed using commercial CFD package Fluent (version 6.3).

2. Mathematical model

The model developed here is a three dimensional, steady state, non-isothermal, single phase model for a single channel of a fuel cell with channel (ducted) cathode design. The continuity, momentum, energy and species equations are solved along the electrochemical equations and membrane equations for obtaining the solution.

2.1. Model assumptions

The following are the assumptions made for the numerical solution of the present model:

a) The water exists as vapor throughout the computational domain.
b) The entropic heat generation and irreversible heat generation in the cathode catalyst layer only is taken into account in the energy source term.
c) Gases are assumed to be ideal and ideal-gas mixing law is used for mixture properties like viscosity and thermal conductivity.
d) The membrane is considered as solid in the model and the water transport across the model is taken into account using empirical relations available in literature.
e) A constant value for contact resistance is assumed for all the channel dimensions considered in the model.

2.2. Fuel cell geometry and computational domain

The fuel cell geometry and the computational domain used in the model are shown in Fig. 1. The fuel cell geometry consists of

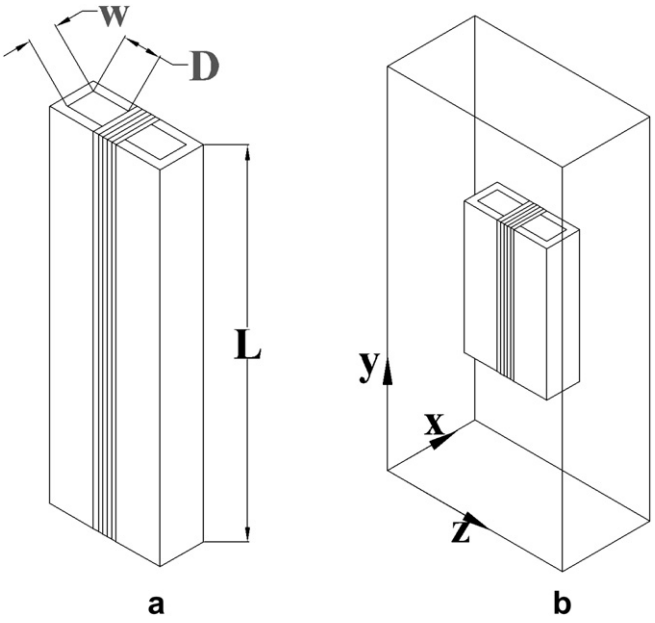

Fig. 1. Fuel cell geometry and computational domain.

anode and cathode flow field plates, flow channels, GDL layers, catalyst layers and the electrolyte membrane. The design and operating parameters used in the study are similar to that given by Tabe et al. [16] and are given in Tables 1 and 2. Since the flow taking place on the cathode side is due to buoyancy, the velocities at the inlet of the cathode are unknown. To take this into account, an extended computational domain is considered in the present study. The domain is extended so that atmospheric conditions prevail on the extended domain boundaries. The computational domain consists of the fuel cell along with the extended domain.

2.3. Governing equations and boundary conditions

The complete fuel cell model can be divided into three subcategories namely a) Flow/Transport submodel, b) Membrane submodel and c) Electrochemical submodel. The governing equations for each of these submodels are given below.

2.3.1. Flow/transport submodel

The governing equations are based on mass, momentum, energy and species conservation and include the applicable source terms.

Table 1
Fuel cell design parameters.

Cell height, L (mm)	15, 30, 45
Gas channel depth, D (mm)	2, 6, 10
Gas channel width, W (mm)	2, 4, 6
Rib width (mm)	1
Anode GDL thickness (mm)	0.54
Cathode GDL thickness (mm)	0.54
Anode catalyst layer thickness (mm)	0.01
Cathode catalyst layer thickness (mm)	0.01
Membrane thickness (mm)	0.051
Porosity of anode GDL/catalyst	0.6/0.4
Porosity of cathode GDL/catalyst	0.6/0.4
GDL/Catalyst layer permeability (m^2)	1e-12
$R_{contact}$ (Ω cm^2)	0.25
V_{oc} (V)	0.92

Table 2
Operating parameters.

Ambient temperature (°C)	20
Ambient relative humidity (%)	30
Temperature of hydrogen (°C)	20
Relative humidity of hydrogen (%)	0
Pressure at anode inlet (atm.)	1
Hydrogen stoichiometry	2.5

Additional buoyancy term has to be included in the momentum equation due to natural convection flow on the cathode side of the cell. The porous nature of the GDL and catalyst layers are taken into consideration by using additional source terms in the momentum equation in the standard fluid flow equations. Only Darcy's viscous resistance term is considered in the source term as the inertial resistance term can be neglected since the velocities are very low. Oxygen and hydrogen are consumed during the electrochemical reactions taking place at the cathode and anode catalyst layers respectively and water vapor is formed at the cathode catalyst layer during the electrochemical reaction. These are included as source/sink terms in the respective species transport equations. The governing equations are as follows:

$$\text{Continuity}: \ \nabla\cdot(\rho v) = S_m \tag{1}$$

The source term for continuity is applicable only for the catalyst region.

$$\text{Anode catalyst layer}: \ S_m = -\frac{I}{2F}M_{H_2} - \frac{\alpha I}{F}M_{H_2O} \tag{2}$$

$$\text{Cathode catalyst layer}: \ S_m = -\frac{I}{4F}M_{O_2} + \frac{(1+2\alpha)I}{2F}M_{H_2O} \tag{3}$$

In all the other zones, i.e., in channel, GDL and membrane, $S_m = 0$.

$$\text{Momentum}: \ \frac{1}{\varepsilon^2}\nabla\cdot(\rho v v) = -\nabla p + \frac{1}{\varepsilon}\nabla\cdot(\mu\nabla v) + \rho g + S_{mom} \tag{4}$$

The source term is applicable only for porous medium where Darcy's viscous resistance term is included. Due to very low flow rates, the inertial loss is considered to be negligible. The source term is thus given by,

$$S_{mom} = -\frac{\mu v}{\beta} \tag{5}$$

In other zones, i.e., in channel and membrane, $S_{mom} = 0$

$$\text{Species}: \ \nabla\cdot(\rho v Y_i) = -\nabla\cdot J_i + S_i \tag{6}$$

where, species flux is given by,

$$\vec{J}_i = -\rho D_{i,j}^{eff}\nabla Y_i \tag{7}$$

and

$$D_{i,j}^{eff} = \varepsilon^{1.5}\left(\frac{P_0}{P}\right)^{1.0}\left(\frac{T}{T_0}\right)^{1.5}D_{i,j}^{ref} \tag{8}$$

The source terms are applicable only to the catalyst layer and are as given below:

$$\text{Hydrogen source term at anode catalyst layer:} \ S_{H_2} = -\frac{I}{2F}M_{H_2} \tag{9}$$

$$\text{Water source term at anode catalyst layer}: \ S_{H_2O,a} = -\frac{\alpha I}{F}M_{H_2O} \tag{10}$$

Oxygen source term at cathode catalyst layer : $S_{O_2} = -\frac{I}{4F}M_{O_2}$

Water source term at cathode catalyst layer : (11)

$$S_{H_2O,c} = \frac{(1+2\alpha)I}{2F}M_{H_2O} \quad (12)$$

In other zones, i.e., channel, GDL and membrane, $S_i = 0$.

$$\text{Energy} : \nabla\cdot(\rho c_p v T) = \nabla\cdot(k_{eff}\nabla T) + S_h \quad (13)$$

S_h is the heat source and is applicable at the cathode catalyst only and is given by,

$$S_h = \left(-\frac{T\Delta S}{4F} + V_{act}\right)I \quad (14)$$

In other zones, i.e., channel, GDL and membrane, $S_h = 0$.

2.3.2. Membrane submodel

A thorough study of water transport in the membrane was done by Springer et al. [31]. The water transport in the membrane is due to: (i) electro-osmotic drag, which is due to protons carrying some water molecules along with them as they move from anode to cathode and (ii) back diffusion, which is due to difference in water concentration across the polymer membrane. Taking both these phenomena into account the net water transport coefficient (α) across the membrane is given as:

$$\alpha = n_d - F\cdot D_w\cdot\frac{(C_{w,c} - C_{w,a})}{I\cdot t_{cat}\cdot t_{mem}} \quad (15)$$

The water transport due to differential pressure across the membrane is not considered in the model as the pressures on both the anode and cathode side are equal to one atmosphere pressure.

The membrane water content, and thus the electro-osmotic and diffusion coefficients, can be calculated using the activities of the gas in the anode and cathode:

Activity,

$$a = \frac{P_{H_2O}}{P_{sat}} \quad (16)$$

The water content in the membrane is calculated using the expression:

$$\lambda = \begin{cases} 0.043 + 17.81a - 39.85a^2 + 36a^3, & 0 < a \le 1 \\ 14 + 1.4(a-1), & 1 < a \le 3 \end{cases} \quad (17)$$

The electro-osmotic drag coefficient 'n_d' and the water diffusion coefficient 'D_w' are calculated using the expressions:

$$n_d = 0.0029\lambda^2 + 0.05\lambda - 3.4\times10^{-19} \quad (18)$$

$$D_w = D_\lambda\, exp\left(2416\left(\frac{1}{303} - \frac{1}{T_c}\right)\right) \quad (19)$$

where,

$$D_\lambda = \begin{cases} 10^{-6}, & \lambda < 2 \\ 10^{-6}(1+2(\lambda-2)), & 2 \le \lambda \le 3 \\ 10^{-6}(3-1.67(\lambda-3)), & 3 < \lambda < 4.5 \\ 1.25\times10^{-6}, & \lambda \ge 4.5 \end{cases} \quad (20)$$

The water concentration at the membrane surfaces of anode and cathode is a function of membrane water content and is given by:

$$C_w = \frac{\rho_{m,dry}}{M_{m,dry}}\lambda \quad (21)$$

The membrane conductivity is calculated using the following expression:

$$\sigma_{mem} = [0.514\lambda - 0.326]\, exp\left[1268\left(\frac{1}{303} - \frac{1}{T}\right)\right] \quad (22)$$

2.3.3. Electrochemical submodel

The reversible voltage of a fuel cell depends on the temperature, pressure and composition of the reactants and is given by the Nernst equation as:

$$E = E^0 + \frac{RT}{2F}\ln\left(\frac{P_{H_2}P_{O_2}^{0.5}}{P_{H_2O}}\right) \quad (23)$$

Due to internal currents and cross-over losses the open circuit potential, V_{oc}, is always less than the reversible voltage. When current is drawn from a fuel cell there are some inherent voltage losses such as activation, ohmic and concentration losses that are always present and are given by:

$$V_{act} = \frac{RT}{\alpha_c F}\ln\left(\frac{i}{i_{o,c}}\right) \quad (24)$$

$$V_{ohm} = \left(R_{cell} + \frac{t_{mem}}{\sigma_{mem}}\right)I \quad (25)$$

$$V_{conc} = \frac{RT}{nF}\ln\left(1 - \frac{i}{i_{lim}}\right) \quad (26)$$

where,

$$i_{lim} = \frac{4FC_{O_2,\infty}}{\frac{t_{gdl}}{D_{O_2}^{eff}} + \frac{1}{h_{m,O_2}}} \quad (27)$$

Because of these inherent voltage losses that are present in a fuel cell during its operation, the operating voltage of a fuel cell is always less than the open circuit voltage and is given by:

$$V_{cell} = V_{oc} - V_{act} - V_{ohm} - V_{conc} \quad (28)$$

Boundary conditions:

$$\text{At anode inlet} : \dot{m}_{H_2} = \frac{I}{2F}S_{H_2},\ Y_{H_2} = 1,\ Y_{H_2O} = 0,\ T_{an,in} = T_{atm}$$

$$\text{At the extended boundary} : Y_{O_2} = Y_{O_2,atm},\quad Y_{H_2O} = Y_{H_2O,atm},\quad T = T_{atm}$$

2.4. Solution strategy

Continuity, momentum, species and energy equations, along with the equations for water transport through the membrane and electrochemical equations were solved simultaneously to obtain the results. The model was solved using commercial CFD software Fluent (version 6.3) which takes into account the porous nature of the computational domain. For solving the water transport equation in the membrane and the electrochemical equations separate user defined function was written. The coupled set of equations was solved iteratively until the scaled residuals for all variables reached a convergence value of 10^{-8}. The solution procedure involves taking the average current density as input, solving for the various overpotentials to obtain the operating cell voltage and hence the polarization curve of the cell. The performance of the cell is presented in terms of the polarization curve and the power density curve.

3. Results and discussion

3.1. Grid independence and extended domain study

Fig. 2 shows the grid independence study conducted for the model. The plot is for the cell with cathode channel dimensions of 2 mm width, 6 mm depth and 45 mm height and for a current density of 100 mA/cm^2. Grid was refined in steps to obtain a final computational grid of 858,700 cells, refinement beyond which the computational results were not affected.

Fig. 3 shows the effect of extended domain on the model solution. Atmospheric temperature and humidity boundary conditions were applied to the extended domain boundary. Fig. 3 shows that when the extended boundary is three times the cell height the boundary conditions at the extended boundary didn't affect the model solution. Therefore the extended domain was chosen to be three times the cell height for further parametric studies.

3.2. Model comparison

The three dimensional model results are compared with the experimental results of Tabe et al. [16] and are shown in Fig. 4. The results show that the model results match well with that of experimental results in the activation overpotential region and in the ohmic overpotential region. The model predicts higher limiting current densities compared to the experimental results. The deviation at high current densities may be due to the liquid water formation in the cell which is not accounted in the model.

3.3. Effect of channel width and depth

Fig. 5(a)–(c) shows the effect of channel depth on the performance of an air-breathing fuel cell for channel widths of 2 mm, 4 mm and 6 mm respectively. The channel height considered for the study is 45 mm.

Fig. 5(a) shows the effect of channel depth on the cell performance for a channel width of 2 mm. It can be seen from the figure that the performance was limited to very low current densities (≈190 mA/cm^2) for a channel depth of 2 mm. The buoyant force is not enough to overcome the resistance offered by the channel for the flow. Where as, with channel depth of 6 mm and 10 mm flow can easily take place through the channel and hence the cell operates at high current densities. There is not much difference in the performance when the channel depth is 6 mm and 10 mm. Fig. 5(b) shows the effect of channel depth on the cell performance for a channel width of 4 mm. For a channel depth of 2 mm the limiting current density is low (≈385 mA/cm^2). At high current densities the buoyancy is not enough to push the flow through the channels. Cell with 6 mm channel depth performs better compared to 10 mm deep channel. This is due to low activation overpotential and lower concentration overpotential. Cell with 6 mm channel depth offers more resistance for the air flow compared to 10 mm channel depth due to smaller hydraulic diameter of the channel. Since the amount of air that is flowing is less for the cell with 6 mm channel depth, the amount of heat carried away will be less. Hence the cell temperatures are high for 6 mm depth channel and the activation overpotential is low. At high cell temperatures, the species diffusivities are high. Hence the mass transfer coefficient is high and the concentration overpotential is low. Fig. 5(c) shows the effect of channel depth on the cell performance for a channel width of 6 mm. The performance is similar to that of 4 mm wide channel.

Maximum power density obtained with a channel width of 2 mm is 210 mW/cm^2 for a channel depth of 6 mm. For a channel width of 4 mm, the peak power density obtained is 240 mW/cm^2 for a channel depth of 6 mm. Similarly for channel width of 6 mm, the peak power density obtained is 240 mW/cm^2 for a channel depth of 6 mm. For a given channel depth, the performance improved with increase in channel width. The limiting current density was improved from 190 mA/cm^2 to 430 mA/cm^2 when the channel depth was 2 mm. For channel depth of 6 mm and 10 mm

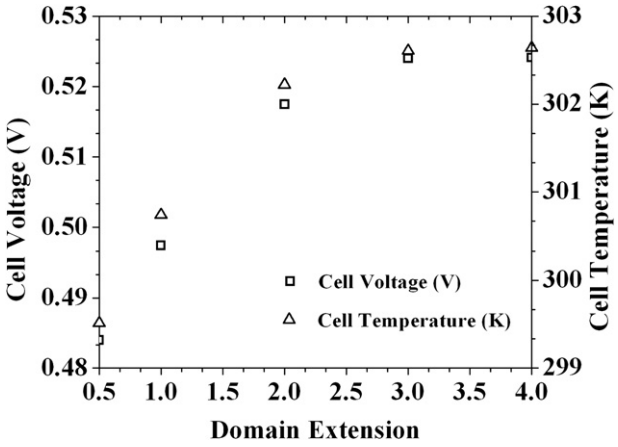

Fig. 3. Effect of extended domain.

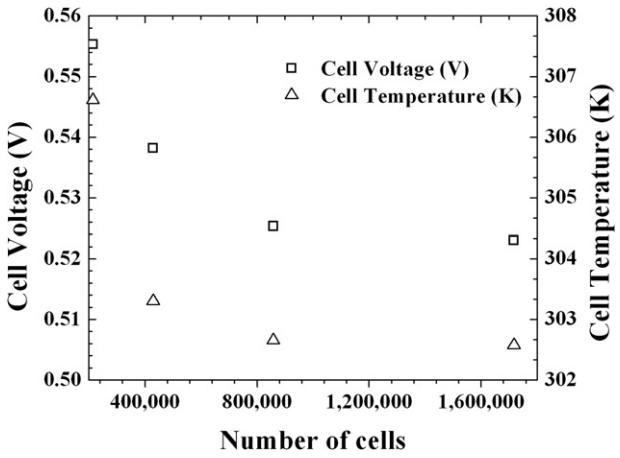

Fig. 2. Grid independence study.

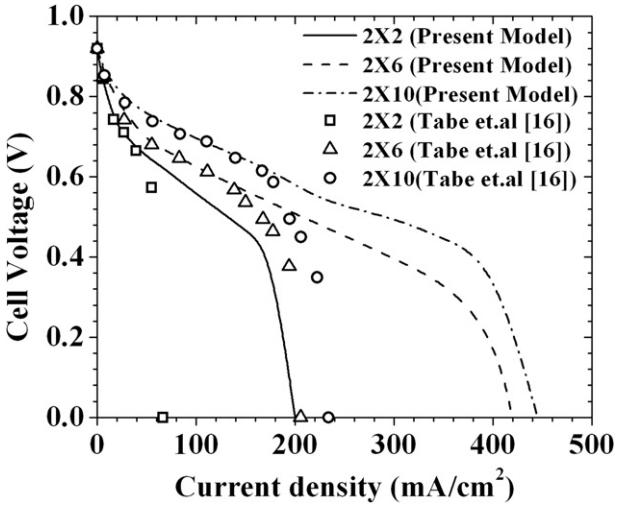

Fig. 4. Model comparison.

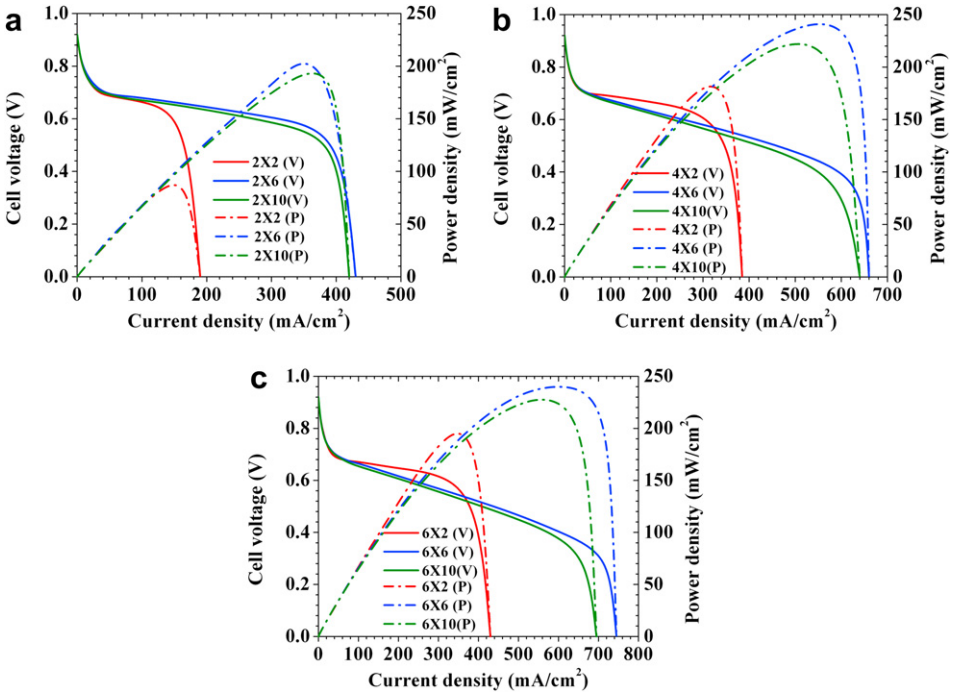

Fig. 5. Effect of channel depth on cell performance.

also the limiting current density increased from 420 mA/cm^2 to 780 mA/cm^2.

Fig. 6(a) shows the variation of oxygen mass fraction in the cathode catalyst layer and GDL–channel interface for a channel with 2 mm width and 2 mm depth and for an average current density of 175 mA/cm^2, close to the limiting current density. Fig. 6 (b) shows the variation of oxygen mass fraction in the cathode catalyst layer and GDL–channel interface for a channel with 2 mm width and 6 mm depth and for an average current density of 400 mA/cm^2 which is close to the limiting current density. In Fig. 6 (a) the mass fractions in the channel and in the GDL–channel interface are nearly equal, whereas in Fig. 6(b) it can be observed that the mass fraction in the GDL–channel interface is larger than the catalyst layer. This shows that in the first case the performance is limited due to the resistance offered by the channel for the buoyancy flow, whereas in the second case the performance is limited due to diffusion resistance offered by the porous media.

For all channel widths, the cell performance is limited due to the flow resistance offered by the channel for a channel depth of 2 mm. Whereas with cathode channel depths of 6 mm and 10 mm and all channel width, the performance is limited due to diffusion resistance offered by the porous media.

3.4. Cell characteristics

Cell characteristics such as local current density distribution, oxygen mass fraction, water vapor mass fraction, temperature difference between the cell and the ambient, oxygen mass transfer coefficient, cathode channel velocity and net water transport coefficient are given. They give better insight about the cell behavior under given operating conditions. The legend in the graphs show the channel dimensions (width × depth) and the average current density for which the graphs are plotted are given in parenthesis.

3.4.1. Current density

Fig. 7 shows the variation of local current density along the cell height.

Fig. 7(a) shows the current density distribution along the cell height for three average current densities and for a channel with 2 mm width and 2 mm depth. The current generation is almost uniform along the height of the channel at low current densities. At high current densities the current generation is more at the bottom of the channel and it decreases along the height of the channel. At the bottom of the channel, where the fresh air enters the channel

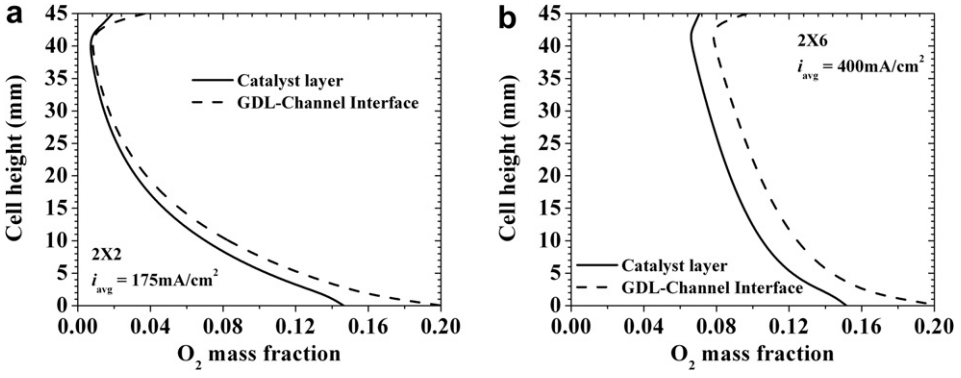

Fig. 6. Mass fraction of oxygen.

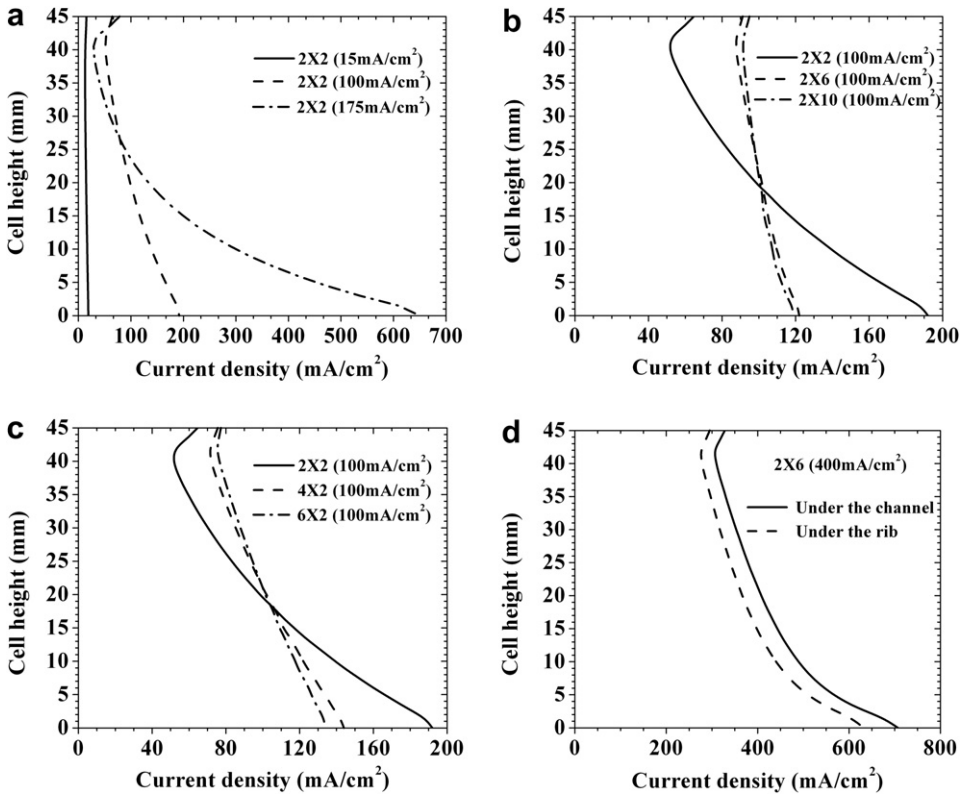

Fig. 7. Current density variation along channel height.

due to buoyancy, oxygen concentration is more and hence the current density is high. As the flow take place along the height of the cell the oxygen concentration decreases due to consumption during the electrochemical reaction and hence the current generation is less. Fig. 7(b) shows the current density variation along the cell height for different channel depths (2, 6, 10 mm). The width of the channel is 2 mm in all the cases. The results plotted are for an average current density of 100 mA/cm^2. The current generation is more non-uniform in the case of 2 mm depth channel. When the channel depths are high, more amount of air and hence oxygen enters the cathode channel. Even though oxygen gets consumed during the electrochemical reaction the oxygen concentration doesn't change much from bottom to the top of the channel and hence the current density is more uniform. Fig. 7(c) shows the effect of channel width on the current density distribution along the height of the fuel cell. It can be seen that the current distribution is more uniform with large channel widths. With larger channel width more the amount of oxygen enters the channel and hence more uniform the current density distribution. Fig. 7(d) shows the current generation from the portion of the catalyst layer beneath the channel and that is beneath the rib. The results given are for a 2 mm width and 6 mm depth channel and for an average current density of 400 mA/cm^2. For the portion of catalyst layer lying directly under the cathode channel, oxygen can easily diffuse and reach the catalyst layer. Where as for the portion of catalyst layer which lay below the ribs the oxygen has to diffuse laterally and reach the catalyst layer. Hence the oxygen concentration is high for the portion of catalyst layer lying just below the channel and hence the current generation is also high.

3.4.2. Oxygen mass fraction

Fig. 8 shows the variation of oxygen mass fraction along the channel height.

Fig. 8(a) shows the variation of oxygen mass fraction along the cell height for different current densities. The variation is more uniform along the cell height at low current densities and the non-uniformity increases with increase in current density. Fig. 8(b) shows the oxygen mass fraction variation for different channel depths at an average current density of 100 mA/cm^2. For a 2 mm depth channel the non-uniformity is very high, where as for 6 mm and 10 mm deep channels the mass fraction variation is more uniform. With increase in channel depth more amount of oxygen can enter the cell and hence the mass fraction variations are more uniform. Fig. 8(c) shows the oxygen mass fraction variation along the cell height for different channel widths. The variation is uniform for larger channel width due to more amount of air entering the channel with higher channel width. Fig. 8(d) shows the variation of oxygen mass fraction for the portion of the catalyst layer which comes under the channel and under the rib. The oxygen can easily diffuse and reach the catalyst layer below the channel area and hence higher the mass fraction of oxygen. Where as for the portion of catalyst layer which lie below the rib the oxygen has to diffuse through a long way laterally and then reach the catalyst layer and hence lesser the oxygen mass fraction. The current generated is a strong function of oxygen concentration in the catalyst layer. Hence the current density profiles are very similar to the oxygen concentration profiles.

3.4.3. Mass transfer coefficient

The mass transfer coefficient is calculated using the expression:

$$h_{m,i} = \frac{D_{i,j}\left[\frac{\partial Y_i}{\partial x}\right]_{GDL}}{\left(Y_{i,GDL} - Y_{i,\infty}\right)} \tag{29}$$

Fig. 9(a) shows the variation of average mass transfer coefficient based on average mass fraction of oxygen in the channel with

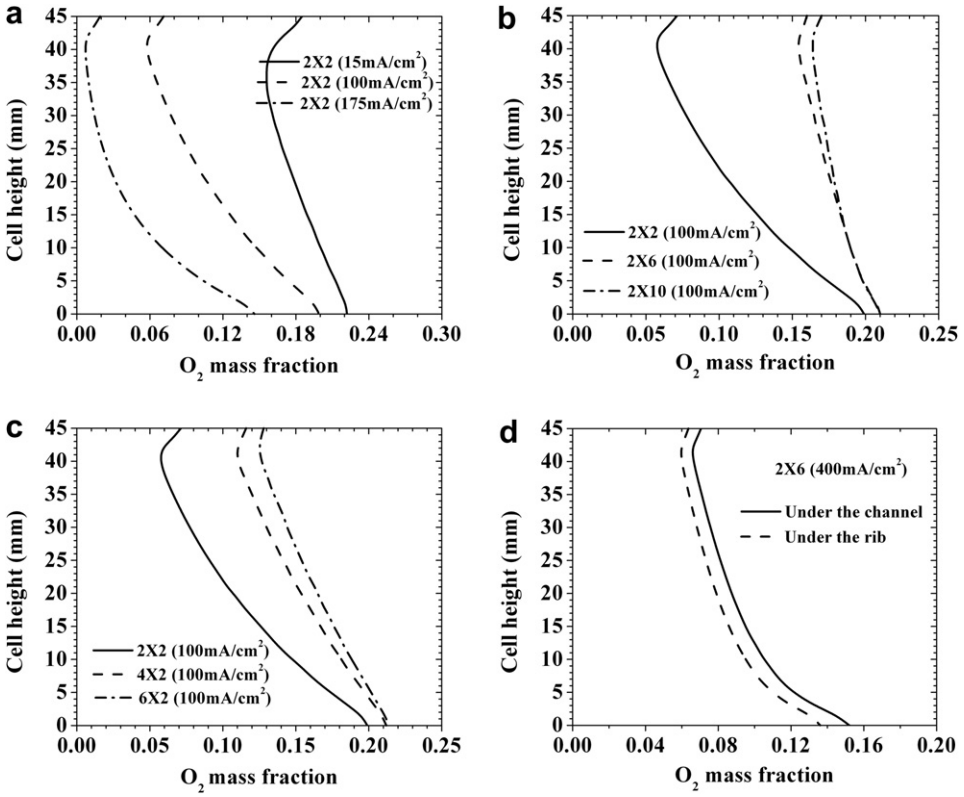

Fig. 8. Variation of oxygen concentration along channel height.

current density for different channel depths. It can be seen that the mass transfer coefficient is high for the cell with cross-section 2 mm × 2 mm. This is because the velocities and the species diffusivities are high for the cell with 2 mm width and 2 mm depth. The amount of air that flow into the channel is less due to small hydraulic diameter of the channel. This small amount of air can carry only a part of the total heat generated and hence the cell temperature is high for the cell with cross-section 2 mm × 2 mm. From equation (8) it can be seen that species diffusivities are a function of temperature, higher the temperature higher the species diffusivities. Since the cell temperature is high, the buoyancy force is high and hence the flow velocities are high. Fig. 9(b) shows the variation of average mass transfer coefficient with current density for different channel widths. There is not much difference in the mass transfer coefficient in this case. Average mass transfer coefficients (0.005–0.025 m/s) are very low in this case due to natural convection on the cathode side, which is one of the reasons why the performance of air-breathing fuel cells are limited to low current densities.

3.4.4. Mass fraction of water vapor

Fig. 10 shows the variation of water vapor mass fraction along the cell height.

Fig. 10(a) shows the variation of water vapor mass fraction for a 2 mm width and 2 mm depth cell at current densities of 15 mA/cm^2, 100 mA/cm^2 and 175 mA/cm^2. Water vapor is generated in the cathode catalyst layer due to electrochemical reactions and hence the water vapor mass fraction increases along the cell height. Higher the average current density, higher the water vapor generated due to the electrochemical reaction and hence the water vapor mass fraction increases with increase in current density as seen in Fig. 10(a). Fig. 10(b) shows the water vapor mass fraction variation along the cell height for a channel width of 2 mm and for three different cathode channel depths. Mass fraction of water vapor is

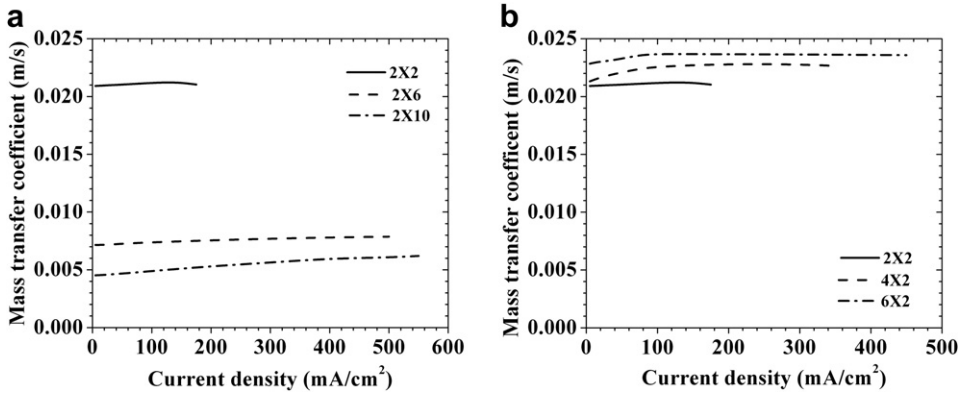

Fig. 9. Variation of oxygen mass transfer coefficient with current density.

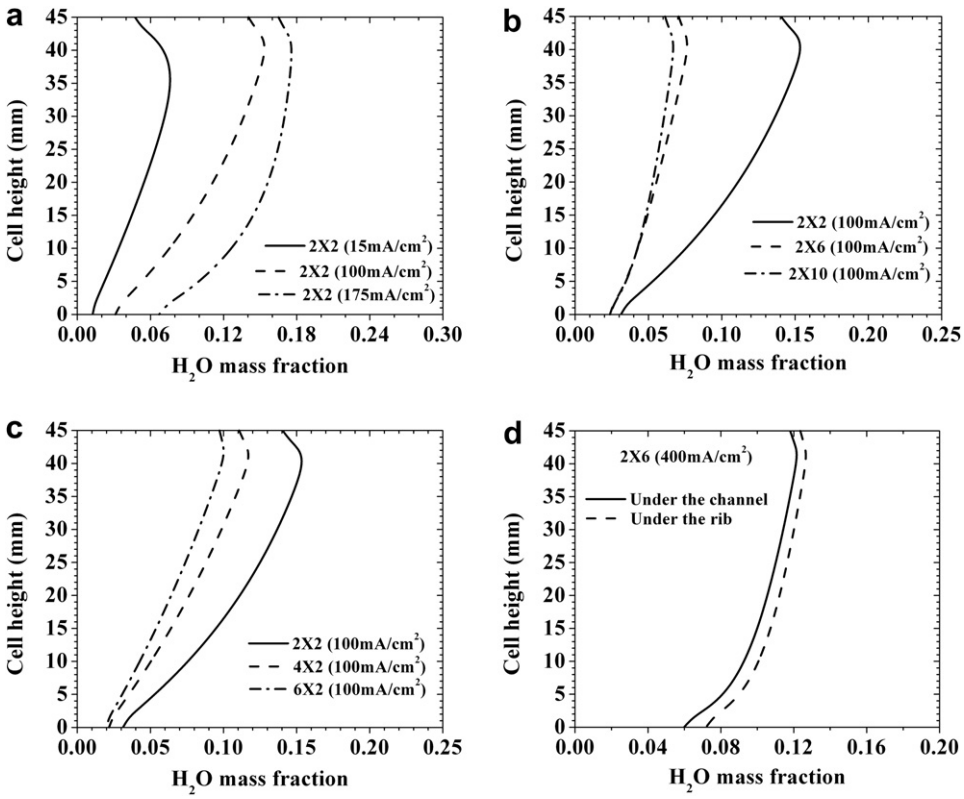

Fig. 10. Variation of water vapor concentration along channel height.

high in the catalyst layer for the cell with 2 mm depth. When the cathode depth is 2 mm the amount of air that enters the cell is less. The water generated due to electrochemical reaction dilutes this small amount of air and hence the mass fraction of water vapor is high in this case. Fig. 10(c) shows the water vapor mass fraction variation for a channel depth of 2 mm and for channel width of 2 mm, 4 mm and 6 mm. When the channel width is more, large amount of air can enter the cell and hence less amount of dilution

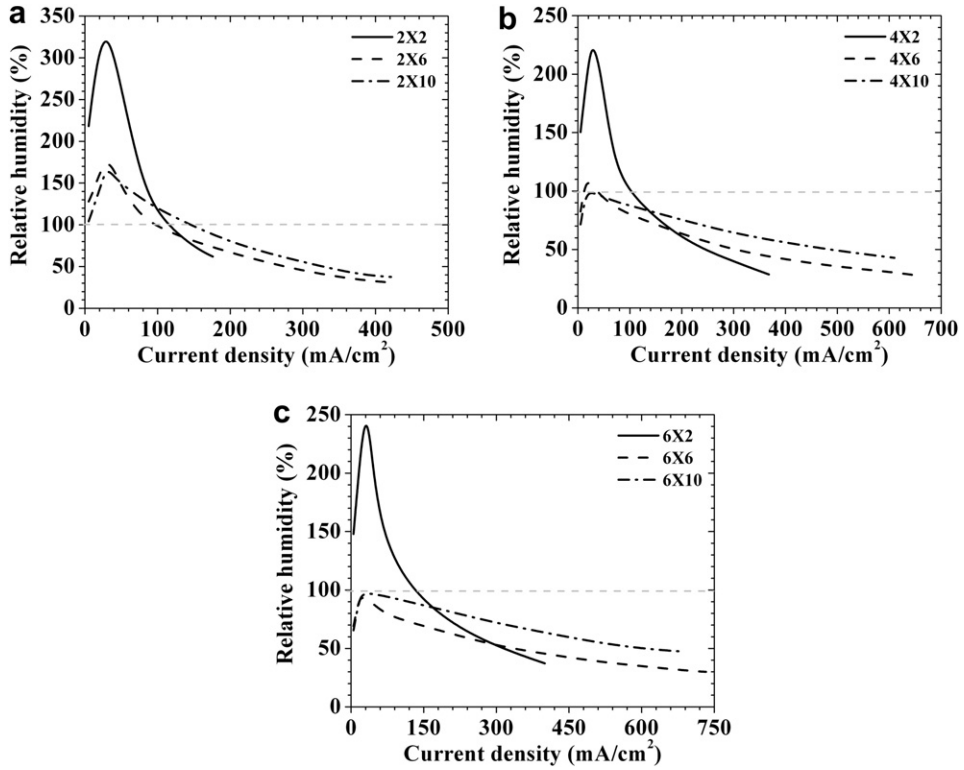

Fig. 11. Relative humidity in the cathode catalyst layer.

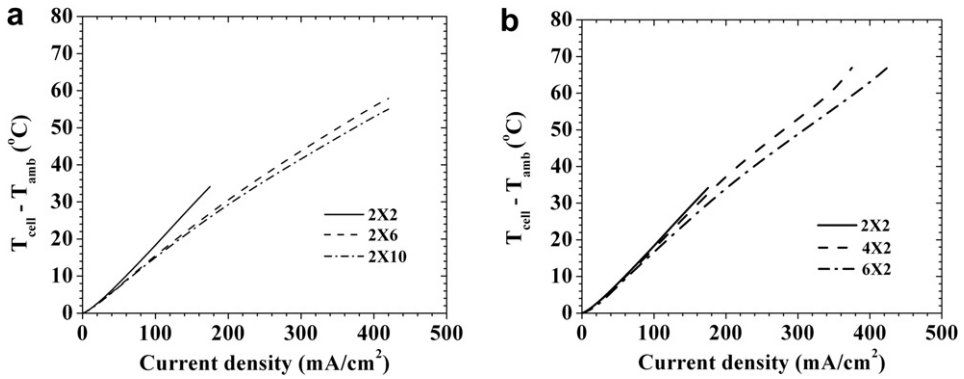

Fig. 12. Temperature difference as a function of current density.

takes place due to water addition. Fig. 10(d) shows the water vapor mass fraction for the portion of the cathode catalyst layer that lay beneath the channel and the rib. The mass fractions are more in the catalyst layer that lay beneath the rib and these are the portions where flooding is likely to happen.

Fig. 11 shows the average relative humidity variation with current density in the cathode catalyst layer for different channel widths and depths. A relative humidity value above 100% means that the partial vapor pressure is above saturation vapor pressure and hence the cell will flood due to liquid water formation. For all the channel dimensions the relative humidity increases with current density at low current densities and then continuously decreases at higher current densities. Both water produced and heat generated increases with increase in current density. At low current densities the water produced dominates the increase in cell temperature and hence the relative humidity increases with increase in current density. Since saturation pressure is a non-linear function of temperature, at high current densities the cell temperatures are so high that the relative humidity continuously decreases at high current densities.

Fig. 11(a) shows the variation in relative humidity for a channel width of 2 mm. When the channel depth is 2 mm, the relative humidities are very high and the chances of cell getting "flooded" are more. The relative humidities are more than 100% for almost the entire operating range of the fuel cell. Whereas, for channel depths of 6 mm and 10 mm "flooding" can happen only at low current densities. The relative humidities are less than 100% at medium and high current densities indicating membrane dehydration to be the major cause limiting the fuel cell performance. Fig. 11(b) shows the variation of relative humidity for a channel width of 4 mm. For channel depth of 2 mm, "flooding" can occur only at low current densities. At high current densities water exists in vapor form as the relative humidity is less than 100%. For channel depth of 6 mm and 10 mm, water exists as vapor in the entire operating range of the fuel cell. Fig. 11(c) shows the relative humidity variation for a channel width of 6 mm. The variation is similar to that of 4 mm wide channel.

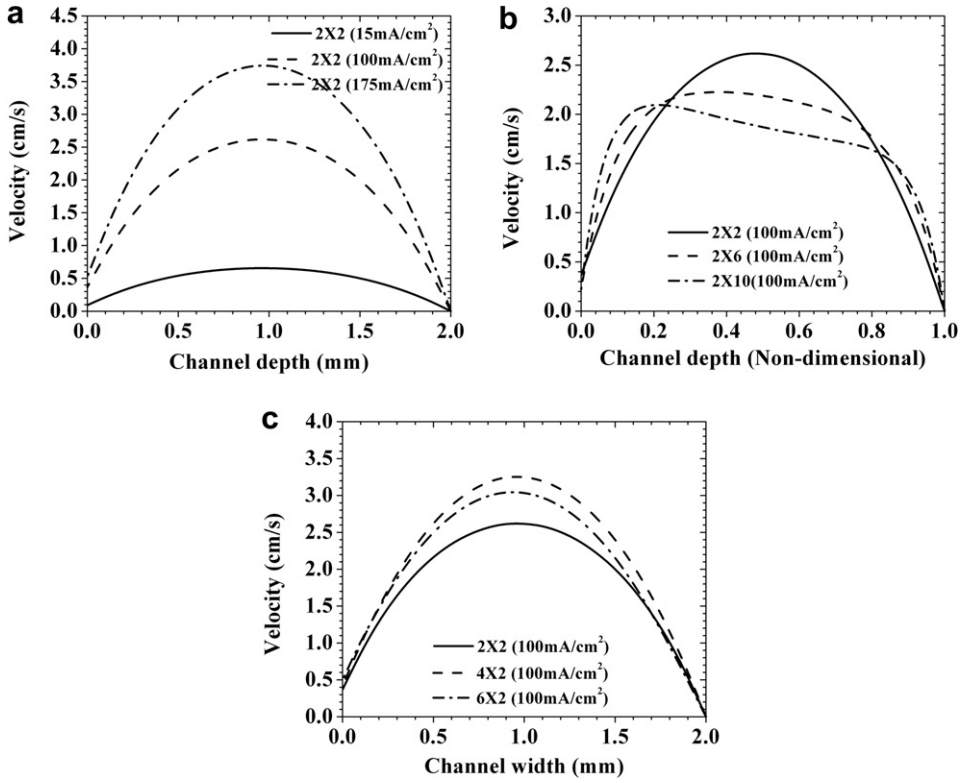

Fig. 13. Cathode channel velocity.

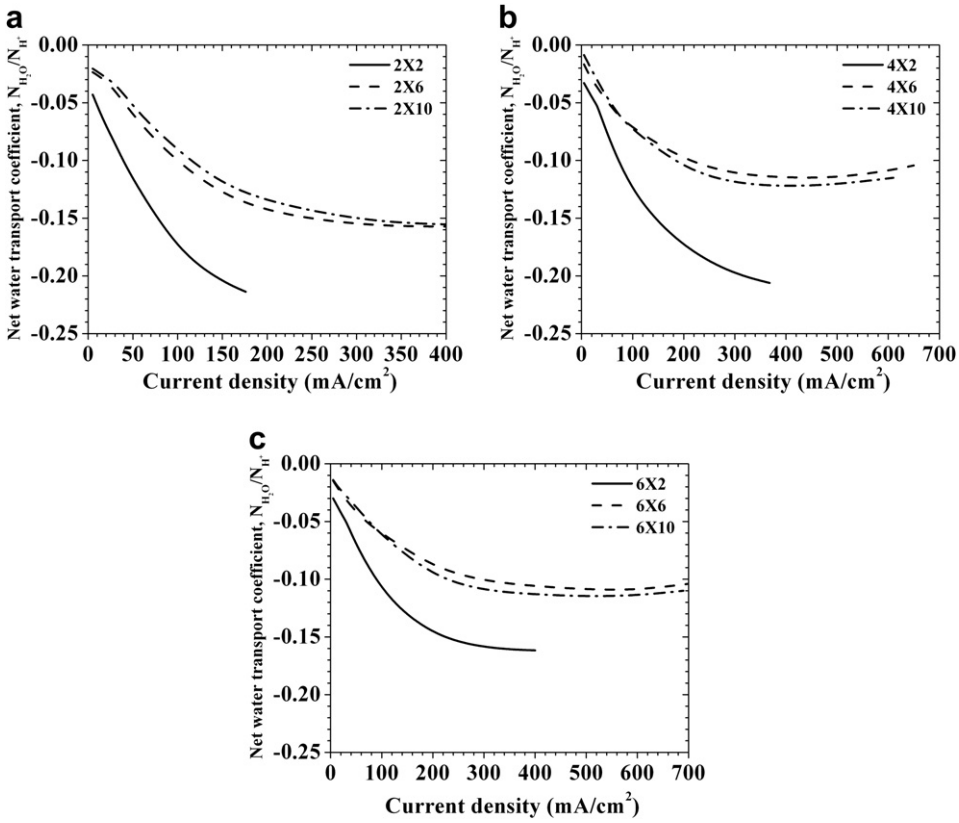

Fig. 14. Net water transport coefficient.

At current densities corresponding to peak power densities, where the cells are expected to operate under practical conditions, the relative humidities are less than 100% and hence cell doesn't flood under those conditions.

3.4.5. *Temperature difference*

Fig. 12 shows the difference between the cell temperature and the ambient as a function of current density. Temperature difference is very important as this is one of the two phenomena that are responsible for buoyancy creation.

Fig. 12(a) shows the difference between the cell temperature and the ambient temperature as a function of current density for different channel depths. As the current density increases, more heat is generated and hence the cell temperature also increases. For the same current density it can be seen that the cell temperature is high for the cell with 2 mm depth. Since the amount of air that enters the channel is less, the heat that can be carried away is low and hence the cell temperature is high. When the channel depth is 6 mm and 10 mm, the amount of air that enters the channel is high and hence can take more amount of heat as it flows along the cathode surface. Because of these reasons the cell temperatures are low for channel depth of 6 mm and 10 mm. Fig. 12(b) shows the temperature difference between the cell and the ambient for different channel widths. In this case also the temperature difference is high for the cell with small channel width. As the channel width increases the activation overpotential decreases and hence

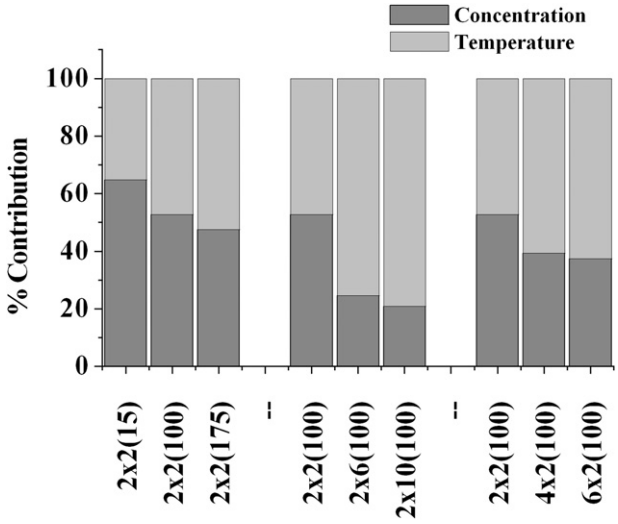

Fig. 15. Relative contribution of driving forces to buoyancy.

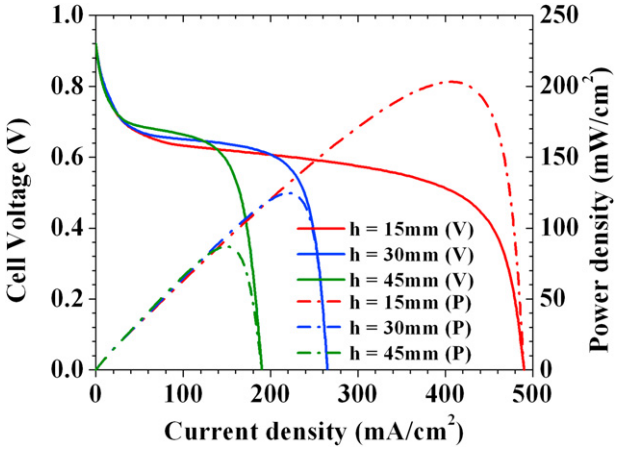

Fig. 16. Effect of cell height.

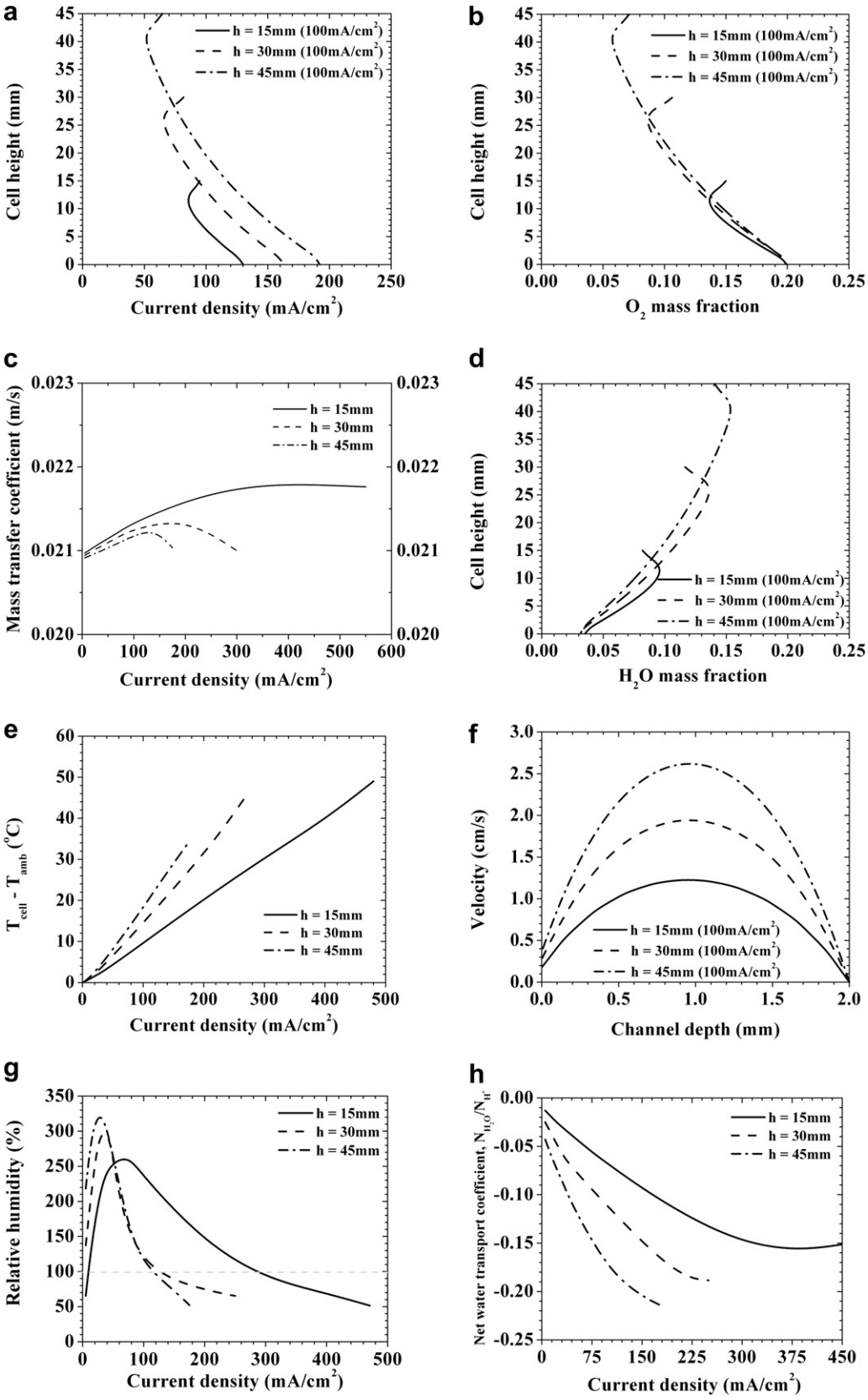

Fig. 17. Cell characteristics.

the irreversible heat generation decreases. Also as the air flow is more, it can take up more heat along with it.

3.4.6. Velocity

Fig. 13 shows the variation of cathode channel velocities at mid height of the channel.

Fig. 13(a) shows the cathode channel velocities for different current densities and for the channel with dimensions 2 mm width and 2 mm depth. The channel velocity increases with current density. At higher current densities the heat generation and the water vapor generated will be high. Thus the buoyancy force induced will be more and hence velocity increases with current density. It can be noticed from the graph that at the left end of the graph which represents the GDL–channel interface the velocities are non-zero indicating flow from the channel to the porous GDL. These velocities are of the order of few millimeters per second. Higher the current density higher is the velocity of flow into the GDL. Fig. 13(b) shows the channel velocities for different channel depths. The results shown are for an average current density of 100 mA/cm^2. For channel depths of 6 mm and 10 mm the velocity boundary layers are still in the developing stage and hence the typical parabolic velocity profile is not visible in this case. Fig. 13(c) shows the channel velocities for different channel widths. In this case the velocity profile is parabolic in nature and hence flow is fully developed. The velocities are higher for wider channels. When the channel width is small the flow resistance offered by the channel will be high due to smaller hydraulic diameter and hence lower the velocity in the channel. The channel velocity is slightly high for 4 mm wide channel than 6 mm wide channel since the cell temperature is slightly high for 4 mm wide channel and hence the buoyancy force is also high.

3.4.7. Net water transport coefficient

Fig. 14 shows the variation of net water transport coefficient with current density. Negative values of net water transport coefficient indicate that the net water transport is from cathode to anode. As the current density increases the more and more water moves from the cathode to the anode side of the fuel cell indicating dominance of back diffusion over the electro-osmotic drag. At very high current densities it can be observed that the net water movement from cathode to anode starts decreasing indicating that the electro-osmotic drag starts to dominate over back diffusion.

3.4.8. Buoyancy forces

Buoyancy force that drives the flow through the cathode channel is due to temperature gradient as well as the concentration gradient between the cell and the ambient. The relative contribution of each of these driving forces is shown in Fig. 15. At lower current densities the buoyancy force is mainly due to concentration gradient, where as at higher current densities the contribution due to temperature gradient is more. When the channel depths are high the driving force is mainly the temperature gradient. As the channel width increases the driving force due to temperature gradient dominates the driving force due to concentration gradient.

3.5. Effect of cell height

Fig. 16 shows the effect of cell height on the performance of an air-breathing fuel cell. The channel width and depth are 2 mm and 2 mm respectively. It can be seen that the performance increases with decrease in cell height. The maximum power density (210 mW/cm^2) obtained is for the shorter cell. As the cell height reduces the limiting current density increases.

3.5.1. Cell characteristics

Fig. 17(a) shows the current density distribution along cell height. The plots are for an average current density of 100 mA/cm^2. As the cell height increases the non-uniformity in current generation increases along the cell height. Fig. 17(b) shows the variation of oxygen mass fraction along cell height for different cell heights. For shorter cells the non-uniformity in mass fraction is less when compared to taller cells. This is because along the channel oxygen gets consumed due to the electrochemical reaction and hence the mass fraction decreases from bottom to top. Fig. 17(c) shows the variation of mass transfer coefficient with current density. There is not much difference in the mass transfer coefficient for different cell heights. Mass transfer coefficient is slightly high for short cells when compared to tall cells. Fig. 17(d) shows the variation of water vapor mass fraction along the cell height. Water vapor mass fraction in the cathode catalyst layer is high for taller cells and hence chances of the cell getting flooded with liquid water also increase with cell height. Fig. 17(e) shows the temperature difference between the cell and the ambient for different cell heights. For the same current density the cell temperatures are high for taller cells when compared to shorter cells. This is because of the difference in current generation in the cell and hence the heat generation. Also the heat and mass transfer coefficients are high for short cells than for tall cells. Fig. 17(f) shows the variation in cathode channel velocity with cell height. Velocities are higher for taller cells as the driving force is high in this case due to larger temperature difference. Fig. 17(g) shows the relative humidity in the cathode catalyst layer for different cell heights. Results show that the cell can flood at low and average current densities. At high current densities close to peak power density, the relative humidities are less than 100% and flooding doesn't occur at those current densities. Fig. 17(h) shows the variation of net water transport coefficient with current density. Negative value of net water transport coefficient indicates net water transport from cathode to anode. As the cell height decreases the amount of water getting transported from cathode to anode decreases.

4. Conclusions

Following conclusions can be drawn from the present study:

1. The results show that the cell performance can be improved by increasing the channel depth, channel width and by reducing the channel height. All the three dimensions significantly affect the cell performance. Increase in channel width may lead to increase in contact resistance. It is recommended to increase the channel depth or decrease the channel height for increasing the cell performance of an air-breathing fuel cell. Cell performance increased when channel depth was increased from 2 mm to 6 mm and then decreased with further increase in channel depth. Therefore there exists an optimum depth of the channel beyond which the performance decreases with increase in channel depth.
2. With a cathode channel depth of 2 mm the performance of the cell is limited by the flow resistance offered by the channel, whereas for channel depths of 6 mm and 10 mm the performance is limited due to channel flow and diffusion resistance offered by the porous media.
3. At low current densities cell is prone to flooding. At current densities corresponding to peak power densities the cell temperatures are very high and hence the cathode side relative humidities are much lesser than the saturation level. At those current densities, at which the fuel cell is expected to operate, ohmic losses due to dehydration of the membrane contribute significantly to the overall voltage loss. Since at medium and

high current densities water exists only in vapor form, a single phase study will be enough to study the performance of an air-breathing fuel cell.

4. Rib width should be smaller for better performance of the cell. Oxygen concentration is low in the catalyst layer portion that lay under the ribs and hence the current generation is also small. Since the water vapor mass fractions are high beneath the rib they are more vulnerable for flooding.
5. Mass transfer coefficients of oxygen at the cathode GDL–channel interface are low (0.005–0.025 m/s) which limit the performance of air-breathing fuel cells to low current densities. Increase in mass transport coefficient at the cathode GDL–channel interface can significantly increase the cell performance.
6. Both temperature and concentration gradient contributes significantly to buoyancy induced flow.

References

[1] T. Fabian, J.D. Posner, R.O' Hayre, S.W. Cha, J.K. Eaton, F.B. Prinz, J.G. Santiago, The role of ambient conditions on the performance of a planar air-breathing hydrogen PEM fuel cell. J. Power Sources 161 (2006) 168–182.

[2] T. Hottinen, O. Himanen, P. Lund, Performance of planar free-breathing PEMFC at temperatures below freezing. J. Power Sources 154 (2006) 86–94.

[3] W. Ying, Y.-J. Sohn, W.-Y. Lee, J. Ke, C.-S. Kim, Three-dimensional modeling and experimental investigation for an air-breathing polymer electrolyte membrane fuel cell (PEMFC). J. Power Sources 145 (2005) 563–571.

[4] T. Hottinen, M. Noponen, T. Mennola, O. Himanen, M. Mikkola, P. Lund, Effect of ambient conditions on performance and current distribution of a polymer electrolyte membrane fuel cell. J. Appl. Electrochem. 33 (2003) 265–271.

[5] B.P.M. Rajani, A.K. Kolar, Heat and mass transfer characteristics in a free breathing fuel cell with a ducted cathode, in: Proceedings of International conference on heat and mass transfer, Sydney, Australia, 2006.

[6] K.P. Manoj, A.K. Kolar, Effect of operating parameters on the performance of an air-breathing PEM fuel cell with a ducted cathode, in: Proceedings of conference on Advances in Energy Research (AER 2006), IIT Bombay, 2006.

[7] R. O'Hayre, T. Fabian, S. Litster, F.B. Prinz, J.G. Santiago, Engineering model of a passive planar air breathing fuel cell cathode. J. Power Sources 167 (2007) 118–129.

[8] S. Litster, N. Djilali, Mathematical modeling of ambient air-breathing fuel cells for portable devices. Electrochim. Acta 52 (2007) 3849–3862.

[9] B.P.M. Rajani, A.K. Kolar, A model for a vertical planar air breathing PEM fuel cell. J. Power Sources 164 (2007) 210–221.

[10] S.U. Jeong, E.A. Cho, H.-J. Kim, T.-H. Lim, I.-H. Oh, S.H. Kim, Effect of cathode open area and relative humidity on the performance of air-breathing polymer electrolyte membrane fuel cells. J. Power Sources 159 (2006) 1089–1094.

[11] S.U. Jeong, E.A. Cho, H.-J. Kim, T.-H. Lim, I.-H. Oh, S.H. Kim, A study on cathode structure and water transport in air-breathing PEM fuel cells. J. Power Sources 158 (2006) 348–353.

[12] S. Sailler, S. Rosini, M.A. Chaib, J.-Y. Voyant, Y. Bultel, F. Druart, P. Ozil, Electrical and thermal investigation of a self-breathing fuel cell. J. Appl. Electrochem. 37 (2007) 161–171.

[13] W. Ying, J. Ke, W.-Y. Lee, T.-H. Yang, C.-S. Kim, Effect of cathode channel configurations on the performance of an air-breathing PEMFC. Int. J. Hydrogen Energy 30 (2005) 1351–1361.

[14] A. Schmitz, M. Tranitz, S. Wagner, R. Hahn, C. Hebling, Planar self-breathing fuel cells. J. Power Sources 118 (2003) 162–171.

[15] Y. Zhang, R. Pitchumani, Numerical studies on an air-breathing proton exchange membrane (PEM) fuel cell. Int. J. Heat Mass Transf. 50 (2007) 4698–4712.

[16] Y. Tabe, S.-K. Park, K. Kikuta, T. Chikahisa, Y. Hishinuma, Effect of cathode separator structure on performance characteristics of free-breathing PEMFC. J. Power Sources 162 (2006) 58–65.

[17] T. Hottinen, O. Himanen, P. Lund, Effect of cathode structure on planar free-breathing PEMFC. J. Power Sources 138 (2004) 205–210.

[18] A. Schmitz, M. Tranitz, S. Eccarius, A. Weil, C. Hebling, Influence of cathode opening size and wetting properties of diffusion layers on the performance of air-breathing PEMFCs. J. Power Sources 154 (2006) 437–447.

[19] T. Hottinen, M. Mikkola, P. Lund, Evaluation of planar free-breathing polymer electrolyte membrane fuel cell design. J. Power Sources 129 (2004) 68–72.

[20] F. Jaouen, S. Haasl, W. van der Wijngaart, A. Lundblad, G. Lindbergh, G. Stemme, Adhesive copper films for an air-breathing polymer electrolyte fuel cell. J. Power Sources 144 (2005) 113–121.

[21] L. Matamoros, D. Bruggemann, Simulation of the water and heat management in proton exchange membrane fuel cells. J. Power Sources 161 (2006) 203–213.

[22] T. Mennola, M. Noponen, T. Kallio, M. Mikkola, T. Hottinen, Water balance in a free-breathing polymer electrolyte membrane fuel cell. J. Appl. Electrochem. 34 (2004) 31–36.

[23] A. Schmitz, S. Wagner, R. Hahn, H. Uzun, C. Hebling, Stability of planar PEMFC in printed circuit board technology. J. Power Sources 127 (2004) 197–205.

[24] Y. Zhang, A. Mawardi, R. Pitchumani, Numerical studies on an air-breathing proton exchange membrane PEM) fuel cell stack. J. Power Sources 173 (2007) 264–276.

[25] D. Chu, R. Jiang, Performance of polymer electrolyte membrane fuel cell (PEMFC) stacks. Part I. Evaluation and simulation of an air-breathing PEMFC stack. J. Power Sources 83 (1999) 128–133.

[26] J.J. Hwang, Species-electrochemical modeling of an air-breathing cathode of a planar fuel cell. J. Electrochem. Soc. 153 (8) (2006) A1584–A1590.

[27] T. Mennola, M. Noponen, M. Aronniemi, T. Hottinen, M. Mikkola, O. Himanen, P. Lund, Mass transport in the cathode of a free-breathing polymer electrolyte membrane fuel cell. J. Appl. Electrochem. 33 (2003) 979–987.

[28] W. Ying, T.-H. Yang, W.-Y. Lee, J. Ke, C.-S. Kim, Three-dimensional analysis for effect of channel configuration on the performance of a small air-breathing proton exchange membrane fuel cell PEMFC. J. Power Sources 145 (2005) 572–581.

[29] L. Matamoros, D. Bruggemann, Concentration and ohmic losses in free-breathing PEMFC. J. Power Sources 172 (2007) 253–264.

[30] Y. Wang, M. Ouyang, Three-dimensional heat and mass transfer analysis in an air-breathing proton exchange membrane fuel cell. J. Power Sources 164 (2007) 721–729.

[31] T.E. Springer, T.A. Zawodzinski, S. Gottesfeld, Polymer electrolyte fuel cell model. J. Electrochem. Soc. 138 (8) (1991) 2334–2342.